Wuhan University
Journal of Natural Sciences

2024, Vol.29 No.6, 579-588

Article ID 1007-1202(2024)06-0579-10 DOI https://doi.org/10.1051/wujns/2024296579

Cite this article: LUAN Xiyu, ZENG Guohui, ZHAO Jinbin, *et al*. Adaptive Control Strategy for Inertia and Damping of Virtual Synchronous Generator Based on CNN-LSTM Data-Driven Model[J]. *Wuhan Univ J of Nat Sci*, 2024, 29(6): 579-588.

Adaptive Control Strategy for Inertia and Damping of Virtual Synchronous Generator Based on CNN-LSTM Data-Driven Model

□ **LUAN Xiyu[1], ZENG Guohui[1], ZHAO Jinbin[2], TIAN Jiangbin[1], ZHANG Zhenhua[1†], LIU Jin[1]**

1. School of Electronic and Electrical Engineering, Shanghai University of Engineering Science, Shanghai 201620, China;

2. Engineering Research Center of Offshore Wind Technology Ministry of Education, Shanghai University of Electric Power, Shanghai 200090, China

Abstract: With the application of distributed power sources, the stability of the power system has been dramatically affected. Therefore, scholars have proposed the concept of a virtual synchronous generator (VSG). However, after the system is disturbed, how to make it respond quickly and effectively to maintain the stability of the system becomes a complex problem.To address this problem, a frequency prediction component is incorporated into the control module of the VSG to enhance its performance. The Convolutional Neural Network-Long Short-Term Memory (CNN-LSTM) model is used for frequency prediction, ensuring that the maximum energy capacity released by the storage system is maintained. Additionally, it guarantees that the inverter's output power does not exceed its rated capacity, based on the predicted frequency limit after the system experiences a disturbance. The advantage of real-time adjustment of inverter parameters is that the setting intervals for inertia and damping can be increased. The selection criteria for inertia and damping can be derived from the power angle oscillation curve of the synchronous generator. Consequently, an adaptive control strategy for VSG parameters is implemented to enhance the system's frequency restoration following disturbances. The validity and effectiveness of the model are verified through simulations in Matlab/Simulink.

Key words: virtual synchronous generator (VSG); adaptive control; frequency restoration; convolutional neural network-long short-term memory (CNN-LSTM)

CLC number: TP203

0 Introduction

Due to the extensive consumption of traditional energy sources, new energy sources have received significant attention. The implementation of distributed energy generation systems has led to various challenges, particularly concerning impact of numerous distributed power sources on the stability of the power system[1-5]. Furthermore, the grid-connected inverters employ a range of control strategies, and the power output of distributed energy resources is subject to fluctuations, which presents a considerable challenge for enhancing the stability of the grid.

To address these issues, scholars have proposed the concept of the Virtual Synchronous Generator (VSG)[6,7].

Received date: 2024-04-06

Biography: LUAN Xiyu, male, Master candidate, research directions: power electronics, artificial intelligence. E-mail: 2589397150@qq.com

† Corresponding author. E-mail: zhenhuazhang1985@163.com

Incorporating inertia and damping into VSG endows them with operational traits akin to those of synchronous generators, leading numerous scholars to delve into extensive research on the control methodologies for VSGs' inertia and damping. Du *et al*[8] proposed a control parameter design by establishing a dynamic model of the power generation system. Ref. [9] introduced an inertial slip control method. Ref. [10] introduced a linear frequency-average small-signal model of the VSG for system analysis and parameter design, outlining the conditions necessary for decoupling the VSG's active power and reactive power control loops. In conclusion, a systematic and incremental approach was recommended for designing the control parameters of the VSG.

In recent years, research on Variable Speed Generator control strategies has increasingly focused on adaptive parameters. Drawing from the characteristics of a second-order system and the deviations in system frequency, Ref. [11] introduced an enhanced control approach that features adaptive inertia and damping. Ref. [12] presented a method for alternating control of inertia and damping to improve system stability. Ref. [13] employed a control strategy aimed at enhancing the transient stability of the power grid by coordinating inertia and damping. The proposed control tactic modifies the virtual inertia and damping coefficients in real time, depending on the current operational frequency deviation and its rate of change. Virtual inertia increases dynamically in the acceleration phase and decreases during deceleration. In contrast, the virtual damping coefficient is elevated, thereby enhancing the positive virtual damping effect throughout the acceleration and deceleration transient processes.

The Bang-Bang algorithm is a relatively straightforward dynamic control strategy[14,15]. In Ref. [14], an enhanced Bang-Bang algorithm was proposed to adaptively adjust the control strategy, switching inertia between large and small values based on varying angular frequencies. Ref. [16] explored adaptive inertia and constant damping control strategies derived from Bang-Bang control, comparing them to a constant parameter VSG. Ref. [17] incorporated fuzzy control into the Bang-Bang algorithm to dynamically adjust virtual inertia. Ref. [18] implemented adaptive damping and established a functional relationship between inertia and the rate of frequency change. This approach effectively addresses the limitations of discontinuous parameter adjustments in the Bang-Bang control algorithm and reduces power fluctuations.

A data-driven modeling method based on Long Short-Term Memory (LSTM) neural networks was proposed[19,20]. Ref. [19] focused on mapping the relationships between electrical quantities and presented a detailed data-driven modeling method for VSG, which was both proposed and verified. In Ref. [21], the Radial Basis Function (RBF) neural network algorithm was utilized to adjust rotational inertia, marking the initial introduction of artificial intelligence algorithms into power electronic control strategies. However, the paper did not provide a specific scheme for controlling the damping coefficients or explore the advantages of RBF neural networks in multi-input systems.

In response to the aforementioned problem, this paper introduces a frequency prediction module to the VSG control system, which forecasts the extreme values of system frequency following abrupt power changes.

Figure 1 shows the framework of an adaptive parameter control model based on data-driven modeling. This model is constructed by analyzing the time series correlations of electrical quantities like voltage, current, and power, revealing their complex interactions to develop an accurate model.

This manuscript employs deep learning algorithms to develop the model. In this study, the CNN-LSTM method is utilized to construct the model, enabling the extraction of multi-dimensional, nonlinear complex data. The data collected under various working conditions are analyzed and trained, ultimately allowing for the prediction of frequency values. Once the expected frequency value is determined, the maximum range of frequency variation can be assessed with greater accuracy. Subsequently, the tuning interval of the parameters can be expanded, leading to the formulation of the final adaptive control strategy based on the power angle characteristic curve.

The remainder of this paper is organized as follows: the first section outlines the methods and principles employed for frequency prediction, the second and third sections present adaptive control strategies and their validation, and the fourth section concludes the paper.

1 Frequency Prediction

A power system's frequency is a crucial indicator of

energy quality. When imbalances occur in the system due to disturbances, accurately predicting the frequency characteristics following the disturbance can aid in controlling the system's response. Deep learning has a wide range of applications across various fields and has significantly enhanced its ability to extract features and make predictions. This paper integrates deep learning with frequency prediction to forecast the system's frequency curve after it has been disturbed.

1.1 Data-Driven Model

Figure 1 illustrates the adaptive parameter control model framework based on data-driven modeling.

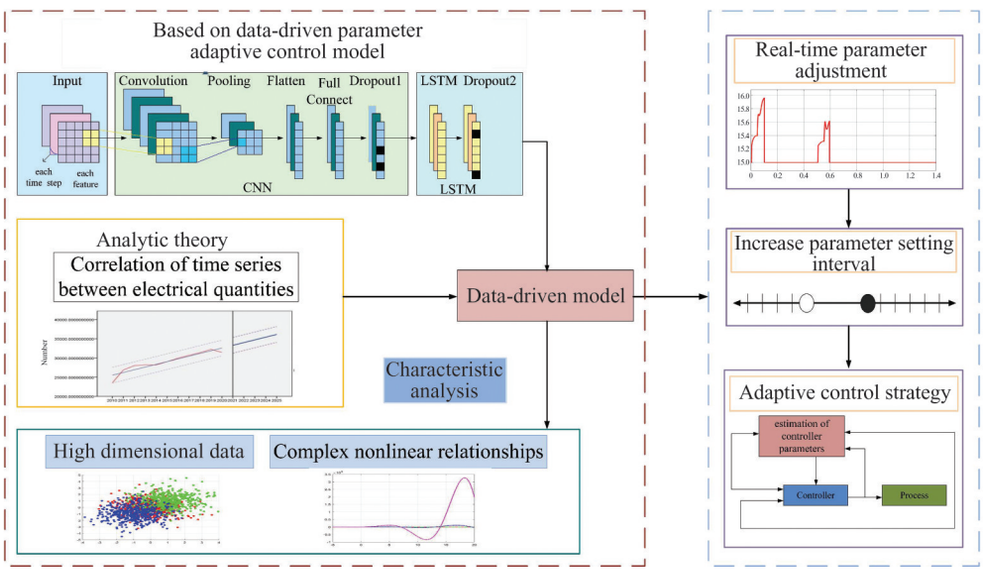

Fig. 1 Adaptive parametric control model based on data-driven modeling

First, data-driven modeling aims to construct a model by analyzing the time series correlations among electrical quantities. In power electronics, these quantities include voltage, current, power, and others, all of which exhibit complex interrelationships. By examining the time series correlations among these electrical quantities, we can uncover their intrinsic relationships, which can then be utilized to develop an accurate model.

1.2 The Principle of CNN-LSTM

The Convolutional Neural Network (CNN) is a network model proposed by LeCun *et al*[22] in 1998. It has found extensive application across various domains, including computer vision and natural language processing.

CNNs are commonly employed for handling large-scale images, where the conventional input format is two-dimensional data. However, in this paper's context, the CNN-LSTM model's input is a multi-dimensional time series.

The network architecture is crafted to operate on one-dimensional data. A one-dimensional convolutional kernel can be visualized as a sliding window that traverses along the time axis to perform sampling. The granularity of each sample can be modified by altering the dimensions of the convolutional kernel.

According to Ref. [23], CNN is typically structured into two primary components: convolutional and classification layers. The filtering layers, which encompass the convolutional and pooling layers, are responsible for processing the input data by filtering, reducing noise and dimensionality, and extracting the necessary features. The classification layers usually consist of multiple fully connected layers. A representative CNN architecture is depicted in Fig. 2, with Conv denoting the convolutional layer, Pooling denoting the pooling layer, and FC denoting the fully connected layer. The basic structure of the CNN-LSTM is shown in Fig. 3.

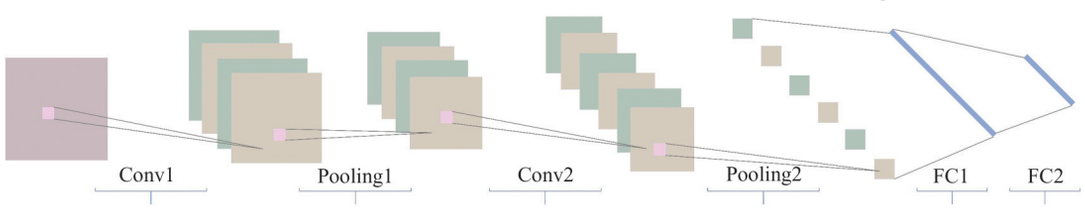

Fig. 2 The structure of CNN

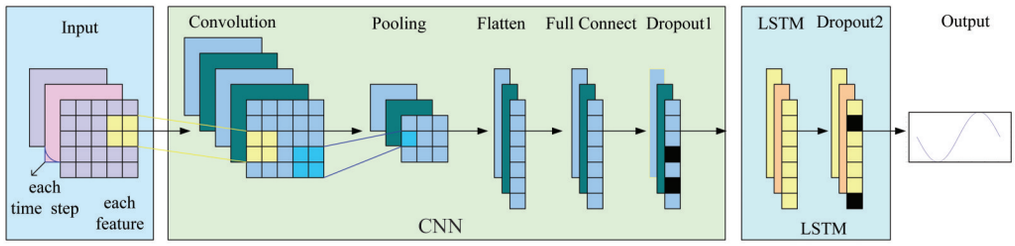

Fig. 3 The structure of CNN-LSTM

Traditional CNNs combine the principles of regional connection and weight sharing. They directly use the original data alternately through convolutional and pooling layers to obtain an adequate representation, enabling the rapid extraction of data features.

1.3 Selection of Input and Output Features

In data-driven modeling, input and output features must be tailored to the specific context of each scenario. Given the constant phase angle relationship between the phases in a three-phase AC power system, this paper focuses on a single phase, utilizing the voltage and current data. It is important to note that once certain features are designated output variables, they should not be reused as input variables. This is because a mapping or functional relationship exists between the input and output variables, and using the same feature for both could lead to redundancy or circularity in the model.

This paper adopts a multi-dimensional input and single-dimensional output approach for frequency prediction. The input features and output features used for frequency prediction are shown in Table 1 and Table 2.

Table 1 Input feature

Input node	Input parameter
1	VSG output current I_a
2	VSG output voltage V_a
3	VSG output active power P
4	VSG output reactive power Q
5	VSG output voltage amplitude instruction E_0
6	VSG output voltage phase Angleinstruction ω_{VSG}

Table 2 Output feature

Condition	Output
The active power rises	Frequency
The negative power rises	Frequency

2 Adaptive Control Strategy for VSG Parameters

2.1 Tuning of Rotational Inertia

When there is an imbalance between the input and output power in the system, the energy storage device provides equivalent rotational inertia to the system through charging and discharging, thereby suppressing power deficits and slowing down the rate of frequency change. If the rotational inertia decreases, the system cannot provide enough inertial support for the frequency. If the rotational inertia rises, although the amplitude of frequency fluctuations is reduced, the overshoot of power will increase, subjecting the energy storage system to more significant power shocks, and the stability of the power system may also be affected. Therefore, it is necessary to set a reasonable range for the value of rotational inertia.

When power imbalances occur in the power system, synchronous generators compensate for power deficits by releasing rotor kinetic energy. Ref. [24] proposed that in frequency variation, only a smaller energy storage capacity is needed to achieve the same frequency regulation capability as synchronous generators. The range of frequency variation in the system is specified to be between 49 and 51 Hz; thus, the maximum kinetic energy[25] released by the synchronous generator is

$$\begin{aligned}\Delta E_{\max} &= \frac{1}{2}J\omega_0^2 - \frac{1}{2}J\left(\frac{50-1}{50}\omega_0\right)^2 \\ &= 0.019\,8J\omega_0^2\end{aligned} \tag{1}$$

In the equation, J represents inertia, ω_0 represents angular velocity. When there is a fluctuation in the system's frequency, the energy storage device requires only an energy capacity of $\Delta E_{\max}$ to emulate the inertial response of a synchronous generator. The storage capacity is adjusted according to the maximum permissible frequency deviation of 1 Hz.

Therefore, the corresponding range of rotational inertia can be obtained based on $\Delta E_{\max}$ as a reference, as

shown in Equation (2).

$$\Delta E_{\max}=\frac{1}{2}J\omega_0^2-\frac{1}{2}J(\frac{50-\nabla f_p}{50}\omega_0)^2$$
$$=\frac{1}{2}J\omega_0^2[1-(\frac{50-\nabla f}{50})^2] \quad (2)$$

In the equation, ∇f_p represents the maximum change in frequency, so when $\nabla f_p<1$ Hz, a larger tuning range is available, as shown in Equation (3).

$$J_{\max 1}=\frac{2\Delta E_{\max}}{\omega_0^2\left[1-\left(\frac{50-\nabla f_p}{50}\right)^2\right]} \quad (3)$$

Since larger values of J result in longer response times, it is necessary to further set the value of J by limiting the adjustment time, as specified in the following section. Therefore, $J_{\max}=\min\{J_{\max 1}, J_{\max 2}\}$.

2.2 Control Strategy for Damping Coefficient

Assuming the rated capacity of a single inverter is $S_N=10\,\text{kV}\cdot\text{A}$, when the frequency of the grid changes by 1 Hz, the active power output of the inverter can vary by a maximum of $\Delta P_{\max}=10$ kW. Based on the principle as mentioned earlier, the initial damping coefficient of the VSG can be determined, as shown in Equation (4).

$$D_P=\frac{\Delta P_{\max}}{\omega_0\Delta\omega_{\max}}=\frac{\Delta P_{\max}}{2\pi\omega_0\Delta f_{\max}}=5\,\text{N}\cdot\text{m}\cdot\text{s}\cdot\text{rad}^{-1} \quad (4)$$

In the equation, $\Delta P_{\max}$ represents the maximum change in active power, $\Delta\omega_{\max}$ represents the maximum change in angular velocity, and $\Delta f_{\max}$ represents the maximum change in frequency. Similarly, this method can ensure that the output power of the inverter does not exceed the capacity limit. However, the set D_P maybe too small, thereby failing to provide sufficient damping power to suppress frequency fluctuations. The predicted actual maximum deviation of frequency is often smaller than the maximum deviation, allowing D_P to be set over a wider range, as shown in Equation (5).

$$D_{\max 1}=\frac{\Delta P_{\max}}{\omega_0\Delta\omega_P}=\frac{\Delta P_{\max}}{2\pi\omega_0\Delta f_P} \quad (5)$$

The Δf_P refers to the maximum deviation in predicted frequency. However, if D_P is too large, the second-order system may transition from under-damped to over-damped, slowing down the system's response speed. Therefore, it is necessary to set another $D_{\max 2}$ for comparison, so $D_{\max}=\min\{D_{\max 1}, D_{\max 2}\}$. Taking the smaller of the two values ensures that the second-order system operates within the under-damped range while also maintaining a faster response speed.

In grid-connected mode, the power grid serves as the power supply that supports the output frequency of the inverter. The simplified topology of the grid connection is shown in Fig. 4, where $E\angle\delta$ is the voltage of the distributed generation, E is the RMS value of the phase voltage, Z is the equivalent impedance, R and X are the equivalent resistance and reactance. $U\angle 0$ is the voltage at the common coupling point. j stands for the imaginary unit.

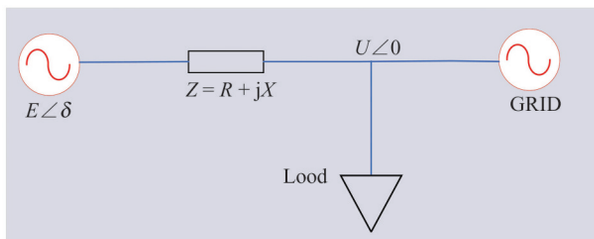

Fig. 4 VSG simplified structure in grid-connected mode

To simplify the analysis, the active and reactive power loops are approximated as decoupled, and it is assumed that the system's equivalent output impedance is inductive. Meanwhile, the influence of the inner loop response on the active power loop and the delay effect in power calculation are ignored. This results in the closed-loop control block diagram of the VSG's output active power, as shown in Fig. 5, where $K_P=3\,EU/X$. 1/s stands for integration operation.

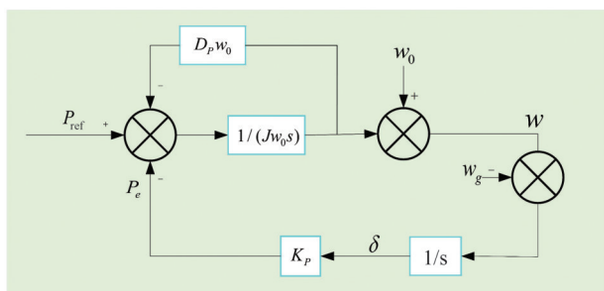

Fig. 5 VSG output power closed-loop

The closed-loop transfer function of the VSG's output power can be obtained, as shown in Equation (6). s stands for the complex variable in the Laplace Transform.

$$G_2(s)=\frac{\Delta P_e}{\Delta P_{\text{ref}}}=\frac{K_P}{J\omega_0 s^2+D_P\omega_0 s+K_p} \quad (6)$$

Equation (6) indicates that it is a typical second-order system, thereby obtaining the damping ratio ξ_g and the settling time t_{sg}, as shown in Eqs. (7) and (8).

$$\xi_g=\frac{D_P}{2}\sqrt{\frac{\omega_0}{K_p J}} \quad (7)$$

$$t_{sg}=\frac{4.4}{\xi_g\omega_{ng}}=\frac{8.8J}{D_P} \tag{8}$$

To ensure that the settling time $t_{sg}<1$s, we stipulat $D_P=5\ \mathrm{N\cdot m\cdot s\cdot rad^{-1}}$. So $J_{max2}=0.56\ \mathrm{kg\cdot m^{-1}}$. In the grid-connected mode, to maintain the power loop in the under-damped range, the damping coefficient D_P should be set to D_{max2}, which is 30 $\mathrm{N\cdot m\cdot s\cdot rad^{-1}}$, as shown in Equation (9).

$$\begin{cases} J_{max}=\min\{J_{max1},0.56\} \\ D_{max}=\min\{D_{max1},30\} \end{cases} \tag{9}$$

This paper stipulates $J_{min}=0.4\ \mathrm{kg\cdot m^{-1}}$, $D_{min}=20\ \mathrm{N\cdot m\cdot s\cdot rad^{-1}}$.

2.3 Adaptive Control Strategy for VSG

When there is a fluctuation in the system power, assume that the active power input steps from P_0 to P_1, the VSG will transit from its original stable operating point a through a transient process to a new stable operating point b. Due to the presence of inertia, the VSG will overshoot point b and reach point c. During this process, the power angle variation of the VSG exhibits decaying oscillations, which can be divided into four intervals: $a\rightarrow b$, $b\rightarrow c$, $c\rightarrow b$, and $b\rightarrow a$, as shown in Fig. 6.

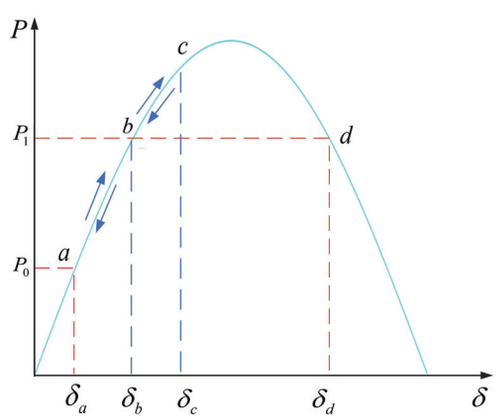

Fig. 6 VSG power angle

During the transient response process of the system, the advantage of the VSG's flexible and adjustable parameters can be utilized to dynamically adjust inertia and damping in real-time based on the changes in physical quantities such as power angle and angular frequency. This optimization aims to improve the transient response. The specific analysis is as follows:

In interval 1, at this point, the virtual rotor angle velocity of the VSG is higher than the grid angle velocity ωg, and the angular velocity is in an acceleration state, $\omega>\omega g$, $\mathrm{d}\omega/\mathrm{d}t>0$. It is necessary to use a larger moment of inertia to suppress $\mathrm{d}\omega/\mathrm{d}t$ while maintaining a smaller damping coefficient to prevent excessive rise in rotational speed leading to overshoot.

In interval 2, although the virtual rotor angle velocity of the VSG is still higher than the grid angle velocity, the angular velocity enters a deceleration state, $\omega>\omega g$, $\mathrm{d}\omega/\mathrm{d}t<0$. A smaller moment of inertia is sufficient to allow the power oscillation to reach point c. At the same time, a larger damping coefficient is used to suppress the rise in the angular frequency deviation $\Delta\omega$. The analysis for intervals 3 and 4 is similar.

Consequently, the magnitude of the moment of inertia and the damping coefficient for the VSG are set based on the discrepancy between the VSG's angular frequency and the grid frequency, along with the rate of change of the angular frequency. The precise relationship is detailed in Table 3.

Table 3 The corresponding relationship between different intervals

Range	$\Delta\omega$	$\mathrm{d}\omega/\mathrm{d}t$	J	D
$a\rightarrow b$	$\Delta\omega>0$	$\mathrm{d}\omega/\mathrm{d}t>0$	J_{max}	D_{min}
$b\rightarrow c$	$\Delta\omega>0$	$\mathrm{d}\omega/\mathrm{d}t<0$	J_{min}	D_{max}
$c\rightarrow b$	$\Delta\omega<0$	$\mathrm{d}\omega/\mathrm{d}t<0$	J_{max}	D_{min}
$b\rightarrow a$	$\Delta\omega<0$	$\mathrm{d}\omega/\mathrm{d}t>0$	J_{min}	D_{max}

According to Table 3 the expressions (10) and (11) for the control strategy can be derived.

$$J=\begin{cases} J_{min}, & \Delta\omega(\mathrm{d}\omega/\mathrm{d}t)\leqslant 0 \\ J_{max}, & \Delta\omega(\mathrm{d}\omega/\mathrm{d}t)>0 \end{cases} \tag{10}$$

$$D=\begin{cases} D_{min}, & \Delta\omega(\mathrm{d}\omega/\mathrm{d}t)\geqslant 0 \\ D_{max}, & \Delta\omega(\mathrm{d}\omega/\mathrm{d}t)<0 \end{cases} \tag{11}$$

3 Simulation Verification

3.1 Frequency Prediction Experiment

3.1.1 Data collection

To obtain more accurate results, this paper first builds a VSG simulation experiment on the Matlab/Simulink platform, with specific basic parameter settings, as shown in Table 4. Two operating conditions are set here: a sudden rise in active power command and a sudden decrease in active power command, thereby obtaining the frequency variation.

As depicted in Fig. 7, at the instance of an abrupt change in the active power command at 1.3 s, the system experiences a disturbance, disrupting the power balance.

Table 4 Basic parameter setting

Parameter	Value
Rated AC voltage U/V	380
Rated AC frequency f_0/Hz	50
Filter capacitor C_f/uF	1
Filter inductance L_f/mH	0.8
J/kg·m²	0.2
D/N·m·s·rad^{-1}	10
Step size (time) /s	0.001
DC side voltage /V	800

In line with the power angle characteristics of a synchronous generator (SG), this disturbance induces oscillations in the system frequency. Such oscillations have the potential to cause damage to system components and compromise the overall stability of the system.

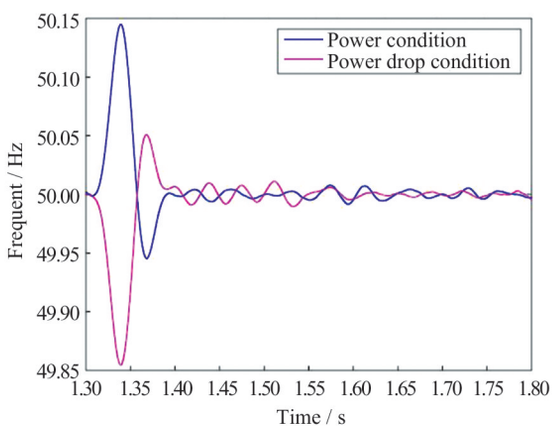

Fig. 7 Frequency variation under different working conditions

3.1.2 Prediction results

In this paper, the CNN-LSTM neural network is employed for modeling, and the frequency change results before and after the active power command change are shown in Fig. 8 and Fig. 9. Two different operating conditions are set, with the active power rising from 4 kW to 10.4 kW at 1.3 s and the active power decreasing from 10.4 kW to 4 kW at 1.3 s. The frequency prediction results and the calculations of Root Mean Square Error (RMSE) and $R2$ (Coefficient of Determination) for these two different operating conditions are presented in Table 5. The experimental results show that the predicted highest and lowest frequency values under the two conditions are close, indicating a good effect and a high overall fitting degree.

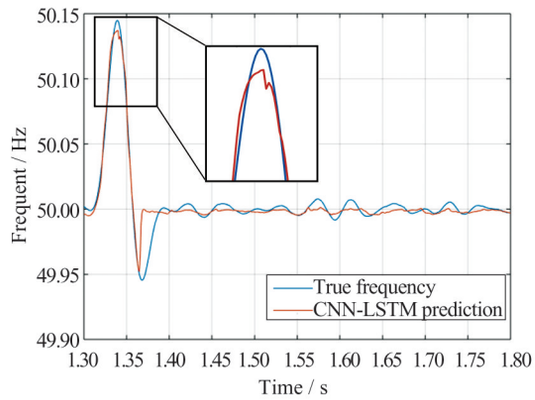

Fig. 8 Power rise prediction results

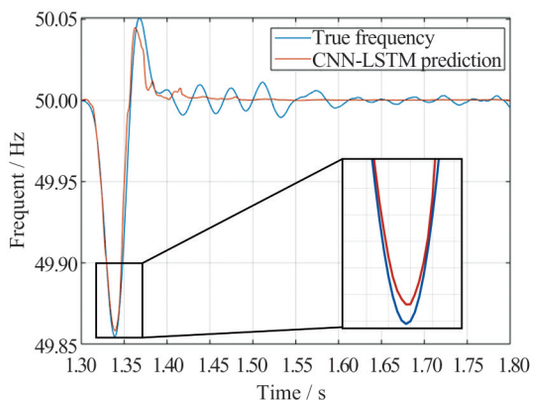

Fig. 9 Power fall prediction results

Table 5 Frequency prediction result

Condition	RMSE	f_{max}/Hz	f_{min}/Hz	$R2$
Fig. 8	0.008 467	50.137 2	49.952 1	0.914 57
Fig. 9	0.006 457	50.044 9	49.858 1	0.952 67

3.2 Adaptive Control Strategy Based on Inertia and Damping

To verify the model's effectiveness under the grid-connected mode, in the case of sudden load rise, the active power command rises from 4 kW to 10.4 kW at 1.3 s. The inertia is taken as $J=0.3\ \text{kg}\cdot\text{m}^2$ and the damping coefficient is taken as $D_P=5\ \text{N}\cdot\text{m}\cdot\text{s}\cdot\text{rad}^{-1}$. Using the obtained predictive model, when the active power suddenly rises to 10.4 kW, the maximum frequency is 50.137 2 Hz. For the adaptive control strategy, taking the maximum value as $J=0.3\ \text{kg}\cdot\text{m}^2$, $\Delta f_P=0.137\ 2$ Hz and substituting it into Equation (3), so $J_{max1}=2.167\ 7\ \text{kg}\cdot\text{m}^2 > J_{max2}=0.56\ \text{kg}\cdot\text{m}^2$, so $J_{max}=0.56\ \text{kg}\cdot\text{m}^2$. Similarly, knowing $\Delta f_P=0.137\ 2$ Hz, substituting it into Equation (5). So $D_{max1}=36.44\ \text{N}\cdot\text{m}\cdot\text{s}\cdot\text{rad}^{-1} > D_{max2}=30\ \text{N}\cdot\text{m}\cdot\text{s}\cdot\text{rad}^{-1}$, so $D_{max}=30\ \text{N}\cdot\text{m}\cdot\text{s}\cdot\text{rad}^{-1}$.

Similarly, in the case of sudden load reduction, the active power command decreases from 10.4 kW to 4 kW at 1.3 s—the constant rotational inertia $J=0.3\ \mathrm{kg\cdot m^2}$, and the damping coefficient $D_P=5\ \mathrm{N\cdot m\cdot s\cdot rad^{-1}}$. Using the obtained predictive model, when the active power suddenly rises to 10.4 kW, the maximum frequency is 50.044 9 Hz. For the adaptive control strategy, taking the maximum value as $J=0.3\ \mathrm{kg\cdot m^2}$, $\Delta f_P=0.044\ 9$ Hz, and substituting it into Eq. (3), so $J_{\max 1}=6.617\ 6\ \mathrm{kg\cdot m^2}>J_{\max 2}=0.56\ \mathrm{kg\cdot m^2}$, so $J_{\max}=0.56\ \mathrm{kg\cdot m^2}$. Similarly, knowing $\Delta f_P=0.044\ 9$ Hz, substituting it into Eq. (5), $D_{\max 1}=111.358\ 6\ \mathrm{N\cdot m\cdot s\cdot rad^{-1}}>D_{\max 2}=30\ \mathrm{N\cdot m\cdot s\cdot rad^{-1}}$, so $D_{\max}=30\ \mathrm{N\cdot m\cdot s\cdot rad^{-1}}$.

We also compared the control strategy of the paper with the results from Ref. [26] and the traditional constant-parameter control strategy. In this paper, the control strategies of J, D and these two parameters are verified. The control results and experimental results are shown in Fig. 10, Fig. 11, Table 6, and Table 7.

For the condition of sudden frequency rises, as shown in Fig. 10, when the active power command rises from 4 kW to 10.4 kW at 1.3 s, it can be seen from Fig. 10(a) and Table 6 that the control method proposed in this paper, compared with the traditional control method and the control method from the reference, has a maximum frequency deviation of 0.079 Hz. In comparison, the maximum frequency deviation in the reference is 0.088 Hz. The proposed method shows better performance in terms of overshoot and responsiveness. On the other hand, the traditional control has a maximum frequency deviation of 0.085 Hz, indicating poor control performance, which leads to larger frequency oscillations. As shown in Fig. 10(b), it can be observed from the comparison that the frequency overshoot of J and D using the adaptive control strategy is smaller than that of J using the adaptive control strategy and D using the adaptive control strategy, and the adjustment time is also improved.

For the condition of sudden frequency decrease, as shown in Fig. 11(a) and Table 7, when the active power command decreases from 10.4 kW to 4 kW at 1.3 s, the control method proposed in this paper exhibits superior performance in terms of overshoot and adjustment time

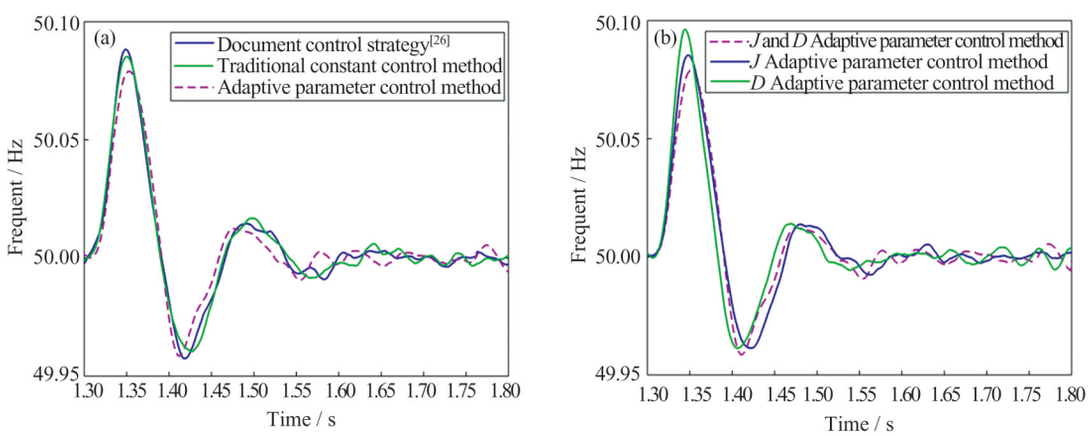

Fig. 10 Comparison of different methods with sudden increase in active power

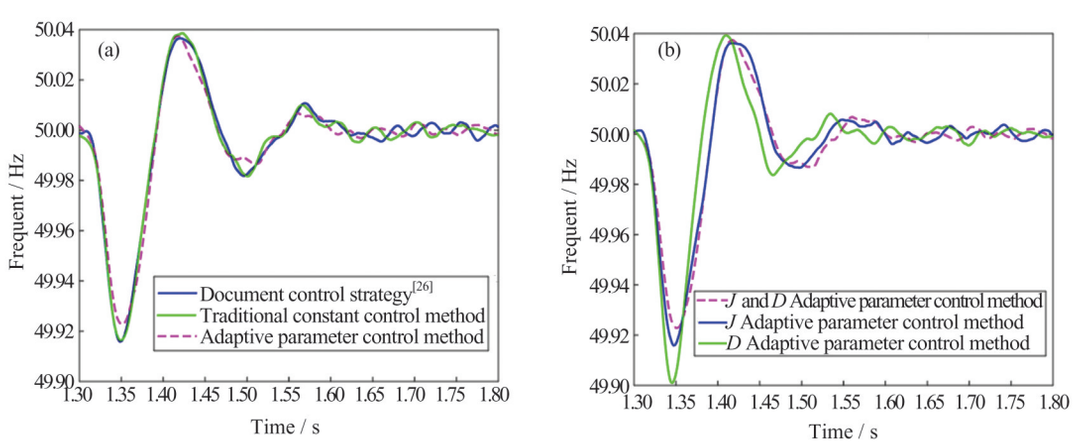

Fig. 11 Comparison of different methods with sudden fall in active power

Table 6 The maximum frequency deviation quantity with sudden increase in active power

Control method	Maximum frequency deviation quantity
Traditional constant control method	0.085
Document control strategy	0.088
J and *D* Adaptive parameter control method	0.079
J Adaptive parameter control method	0.085
D Adaptive parameter control method	0.096

Table 7 The maximum frequency deviation quantity with sudden fall in active power

Control method	Maximum frequency deviation quantity
Traditional constant control method	0.084
Document control strategy	0.084
J and *D* Adaptive parameter control method	0.077
J Adaptive parameter control method	0.085
D Adaptive parameter control method	0.099

compared to the other two methods. The data shows that it performs better in terms of overshoot. It can be observed from Fig. 11(b) that when both *J* and *D* adopt adaptive strategies, the maximum frequency deviation is the lowest, and the overshoot is smaller.

Overall analysis shows that under the grid-connected mode, the proposed adaptive coordination control strategy of inertia and damping enables the VSG's frequency and output active power to recover and stabilize faster, improving the reliability of the system operation. In summary, the parameter adaptive control strategy proposed in this paper can effectively rise the system inertia, provide timely frequency support, and thereby reduce the frequency deviation of low-inertia power grids.

4 Conclusion

This paper proposes a new parameter tuning method that attempts to apply neural networks to parameter tuning and provides a specific scheme for adjustment.

The paper introduces a frequency prediction module based on CNN-LSTM into the VSG model. By predicting the maximum and minimum frequency values after the system is disturbed, it calculates a broader tuning range for rotational inertia and damping coefficient. Furthermore, it takes advantage of the real-time adjustable characteristics of the inverter parameters for tuning. In contrast to the approaches documented in the literature and conventional methods, the proposed strategy can reduce the time required to achieve a steady state following a change in active power, thereby enhancing the system's dynamic response process. The efficacy of the proposed strategy and its theoretical underpinnings are also confirmed through the simulation model developed, leading to an overall enhancement in dynamic performance.

References

[1] Ali N D, Kumar D. Virtual inertia based SVPN sequence control scheme for voltage unbalance mitigation in coordination with DSM on a stand alone microgrid[J]. *Electric Power Components and Systems*, 2023: 1-25. DOI: 15325008.2023.2288703.

[2] Behera S K, Panda A K, Naik N V. Adaptive active and reactive power control strategy for virtual synchronous generator [J]. *International Journal of Circuit Theory and Applications*, 2024, **52**(6): 2635-2654.

[3] Dierkes S, Bennewitz F, Maercks M, *et al*. Impact of distributed reactive power control of renewable energy sources in smart grids on voltage stability of the power system[C]// 2014 *Electric Power Quality and Supply Reliability Conference* (*PQ*). New York: IEEE, 2014: 119-126.

[4] Farmer W J, Rix A J. Impact of continuous stochastic and spatially distributed perturbations on power system frequency stability[J]. *Electric Power Systems Research*, 2021, **201**: 107536.

[5] Liao H F, Zeng G H, Huang B, *et al*. Optimal control virtual inertia of optical storage microgrid based on improved sailfish algorithm[J]. *Wuhan University Journal of Natural Sciences*, 2022, **27**(3): 218-230.

[6] Jain A, Pathak M K, Padhy N P. Conjoint enhancement of VSG dynamic output responses by disturbance-oriented adaptive parameters[J]. *IEEE Transactions on Industrial Informatics*, 2024, **20**(2): 2079-2096.

[7] Li J R, Li H Y, Lim M K, *et al*. Improved artificial jellyfish search algorithm: Virtual synchronous generator control strategy[J]. *Engineering Optimization*, 2024, **56**(6): 854-873.

[8] Du Y, Guerrero J M, Chang L C, *et al*. Modeling, analysis, and design of a frequency-droop-based virtual synchronous generator for microgrid applications[C]//2013 *IEEE ECCE Asia Downunder*. New York: IEEE, 2013: 643-649.

[9] Liu J, Miura Y, Ise T. Comparison of dynamic characteristics between virtual synchronous generator and droop control in

inverter-based distributed generators[J]. *IEEE Transactions on Power Electronics*, 2016, **31**(5): 3600-3611.

[10] Wu H, Ruan X B, Yang D S, *et al*. Small-signal modeling and parameters design for virtual synchronous generators[J]. *IEEE Transactions on Industrial Electronics*, 2016, **63**(7): 4292-4303.

[11] Liu D, Jiang K Z, Ji X T, *et al*. Improved VSG strategy of grid-forming inverters for supporting inertia and damping[J]. *Frontiers in Energy Research*, 2024, **11**: 1331024.

[12] Li D D, Zhu Q W, Lin S F, *et al*. A self-adaptive inertia and damping combination control of VSG to support frequency stability[J]. *IEEE Transactions on Energy Conversion*, 2017, **32**(1): 397-398.

[13] Wang L, Zhou H, Hu X K, *et al*. Adaptive inertia and damping coordination (AIDC) control for grid-forming VSG to improve transient stability[J]. *Electronics*, 2023, **12**(9): 2060.

[14] Li J, Wen B Y, Wang H Y. Adaptive virtual inertia control strategy of VSG for micro-grid based on improved Bang-Bang control strategy[J]. *IEEE Access*, 2019, **7**: 39509-39514.

[15] Deng X M, Lu J N. Bang Bang control of unified chaotic system[J]. *Wuhan Univ J of Nat Sci*, 2003, **8**(1): 311-315.

[16] Elwakil M M, El Zoghaby H M, Sharaf S M, *et al*. Adaptive virtual synchronous generator control using optimized Bang-Bang for Islanded microgrid stability improvement[J]. *Protection and Control of Modern Power Systems*, 2023, **8**(1): 57-78.

[17] Mentesidi K, Garde R, Aguado M, *et al*. Implementation of a fuzzy logic controller for virtual inertia emulation[C]// 2015 *International Symposium on Smart Electric Distribution Systems and Technologies* (*EDST*). New York: IEEE, 2015: 606-611.

[18] Shi R L, Zhang X, Hu C, *et al*. Self-tuning virtual synchronous generator control for improving frequency stability in autonomous photovoltaic-diesel microgrids[J]. *Journal of Modern Power Systems and Clean Energy*, 2018, **6**(3): 482-494.

[19] Tian J B, Zeng G H, Zhao J B, *et al*. A data-driven modeling method of virtual synchronous generator based on LSTM neural network[J]. *IEEE Transactions on Industrial Informatics*, 2024, **20**(4): 5428-5439.

[20] Feng Z X, Ge X, Zhou Y J, *et al*. A power load prediction by LSTM model based on the double attention mechanism for hospital building[J]. *Wuhan Univ J of Nat Sci*, 2023, **28**(3): 223-236.

[21] Yao F J, Zhao J B, Li X J, *et al*. RBF neural network based virtual synchronous generator control with improved frequency stability[J]. *IEEE Transactions on Industrial Informatics*, 2021, **17**(6): 4014-4024.

[22] LeCun Y, Bottou L, Bengio Y, *et al*. Gradient-based learning applied to document recognition[J]. *Proceedings of the IEEE*, 1998, **86**(11): 2278-2324.

[23] Zhi Z, Liu L S, Liu D T, *et al*. Fault detection of the harmonic reducer based on CNN-LSTM with a novel denoising algorithm[J]. *IEEE Sensors Journal*, 2022, **22**(3): 2572-2581.

[24] Liu J, Yao W, Wen J Y, *et al*. A wind farm virtual inertia compensation strategy based on energy storage system[J]. *Proceedings of the CSEE*, 2015, **35**(7):1596-1605(Ch).

[25] Li T Y, Wen B Y, Wang H Y. Adaptive parameter control strategy of virtual synchronous generator based on frequency prediction[J]. *Journal of Fuzhou University*,2020,**48**(6):720-726(Ch).

[26] Yang Y, Mei F, Zhang C Y, *et al*. A novel pulse-source-based method for measuring transfer impedance of high-frequency current sensor[J]. *Electric Power Automation Equipment*, 2019, **39**(3): 125-131(Ch).

基于CNN-LSTM数据驱动模型的VSG转动惯量和阻尼系数的自适应控制策略

栾希宇[1]，曾国辉[1]，赵晋斌[2]，田江斌[1]，张振华[1†]，刘瑾[1]

1. 上海工程技术大学 电子电气工程学院，上海 201620

2. 上海电力大学 海上风电技术教育部工程研究中心，上海 200090

摘要：虚拟同步发电机（VSG）通过提供惯量和阻尼支撑来提高电力系统的稳定性。然而，系统受到干扰后，如何使VSG快速有效地响应以维持系统稳定成为一个难题。为了提升VSG的性能，本文在VSG的控制模块中加入了频率预测模块，CNN-LSTM模型常用于处理时间序列数据，本文使用此模型来预测系统受到干扰后的频率值。本文在满足储能所释放的最大能量不变和逆变器的输出功率不超过额定容量的前提下，基于系统受到干扰后预测频率的极限值，并利用逆变器参数实时调整的优势，增大了惯量和阻尼的参数区间。惯性和阻尼的选择标准通过同步发电机的功角振荡曲线获得。采用的VSG参数的自适应控制策略增强了系统在受到干扰后的频率恢复能力。在Matlab/Simulink中进行了仿真，试验结果验证了模型的合理性和有效性。

关键词：虚拟同步发电机（VSG）；自适应控制；频率恢复；CNN-LSTM

□